ELSEVIER

Solid State Ionics 123 (1999) 209–224

SOLID STATE IONICS

An electrode kinetics study of H_2 oxidation on $Ni/Y_2O_3–ZrO_2$ cermet electrode of the solid oxide fuel cell

S.P. Jiang[a,*], S.P.S. Badwal[b]

[a]*Ceramic Fuel Cells Limited, 170 Browns Road, Noble Park, Vic. 3174, Australia*
[b]*CSIRO, Manufacturing Science and Technology, Private Bag 33, Clayton South MDC, Vic. 3169, Australia*

Received 1 November 1998; accepted 30 March 1999

Abstract

Hydrogen oxidation on Ni/3 mol% $Y_2O_3–ZrO_2$ (Ni/Y-TZP) cermet electrodes has been studied in moist H_2 environments. The impedance behaviour is characterised by two clearly separated arcs in the frequency domain, indicating that the overall electrode reaction is controlled by at least two rate limiting processes in series. The electrode process associated with the low frequency arc is mainly dependent on the H_2 concentration. Moreover, the electrode conductivity of the low frequency arc (σ_L) is independent of temperature and the polarisation potential. Based on these observations, the electrode process associated with the low frequency arc has been attributed to hydrogen dissociative adsorption/diffusion on the surface of Ni particles. The electrode process of the high frequency arc is also affected by the H_2 concentration and by oxygen partial pressure (P_{O_2}), however in contrast to the low frequency arc, the electrode conductivity associated with the high frequency electrode process (σ_H) showed a strong temperature dependence with an activation energy of ~162 kJ mol^{-1} and it increases with increasing polarisation potential. This arc has been attributed to hydrogen transfer from the Ni electrode surface to the Y-TZP electrolyte surface, followed by a charge transfer process on the electrolyte surface near the interface region. The results of this study clearly demonstrate that the Y-TZP in the Ni cermet electrodes has little effect on the reaction mechanism, but plays an important role in modifying the electrode microstructure and kinetics of the fuel oxidation reaction.

Keywords: Cermet electrode; Electrode kinetics; Solid oxide fuel cell; Electrochemical impedance spectroscopy

1. Introduction

$Ni/Y_2O_3–ZrO_2$ (Ni/YSZ) cermets are invariably used as fuel electrodes in solid oxide fuel cells (SOFCs) primarily due to their high electrochemical performance, good chemical stability and low cost [1]. A substantial amount of work has been carried out to optimise the microstructure and the electrical and electrochemical properties of these materials [2–5]. It is widely recognised that the performance of Ni/YSZ cermet electrodes is very much dependent on their method of preparation and the microstructure. Nickel in the cermet plays an important

*Corresponding author. Tel: +61-3-9545-2850; fax: +61-3-9544-1128.

E-mail address: jiang@mst.csiro.au (S.P. Jiang)

0167-2738/99/$ – see front matter
PII: S0167-2738(99)00124-1

catalytic role in the oxidation of hydrogen [3,6]. An understanding of the nature of the fuel oxidation process on Ni/YSZ electrodes is becoming increasingly important as the operation of the solid oxide fuel cell is being driven towards lower operating temperatures (600 to 800°C) due to the high costs of the interconnect material, balance of plant items and corrosion of cell components [7,8].

It has been demonstrated that the electrode activity (i.e. the electrode interface conductivity) for Ni anodes increases with the length of the three phase boundary (TPB, where the electrode, electrolyte and gas phases meet) [9,10], indicating that the rate limiting reaction occurs in a region close to the electrode/electrolyte interface. Our recent studies have demonstrated that the hydrogen oxidation in Ni anodes is controlled by two electrode processes in series: a hydrogen adsorption/diffusion process on the surface of Ni particles and a charge transfer process on zirconia electrolyte surface [11,12]. In moist H_2 (e.g., 98% H_2/2% H_2O), the impedance spectra of Ni and Ni/Y_2O_3–ZrO_2 anodes show the existence of one or more (up to three) arcs [3,10,12–15], suggesting the contribution from several rate limiting processes to the overall H_2 oxidation reaction. The impedance behaviour also points to a dependence of the reaction kinetics and mechanism on the microstructure of the electrode. The important roles of the zirconia phase and cermet preparation methods on the microstructure have been clearly demonstrated [3,4], however there is still uncertainty about the mechanism of H_2 oxidation and especially the role of zirconia–yttria (in the Ni/ZrO_2–Y_2O_3 system) in the overall H_2 oxidation in solid oxide fuel cells [16].

In this paper, the H_2 oxidation on Ni/3 mol% Y_2O_3–ZrO_2 (Ni/Y–TZP) cermet electrodes has been investigated in moist H_2 in the temperature range of 1000 to 800°C by electrochemical impedance spectroscopy and galvanostatic current interruption techniques. The effect of H_2 concentration and partial pressure of oxygen (P_{O_2}) on the oxidation reaction was investigated by changing the H_2 concentration at a constant water content. The role of zirconia in the cermet electrodes has been studied by varying the amount of zirconia content in the cermet electrode.

2. Experimental

The electrolyte discs were prepared from a powder (Tosoh Corporation, Japan) of 3 mol% Y_2O_3–ZrO_2 (abbreviated as Y-TZP) composition. The powder was pressed into discs and sintered at 1500°C for 4 h. The final diameter of the discs was 19 mm and thickness was 0.9 mm. Ni and Ni/Y-TZP electrodes were prepared by milling NiO (Ajax, Australia) and Y-TZP powders in an organic media for several hours, using Y-TZP balls as the grinding media. The pastes were prepared by dispersing the electrode powder in triethylene glycol. The electrode compositions studied were 100% Ni (Ni electrode), 80 vol% Ni+20 vol% Y-TZP (80% Ni/20% Y–TZP) and 70 vol% Ni+30 vol% Y-TZP (70% Ni/30% Y–TZP). The anodes were prepared by slurry painting the electrode paste on one side of the electrolyte discs, followed by firing at 1400°C for 2 h in air. The thickness of the electrode coatings was in the range of 25 to 35 μm. The electrode area was about 0.45 cm^2. Platinum paste (Engelhard No. 6082) was applied on the other side of the electrolyte disc to construct counter and reference electrodes. The counter electrode was in the centre opposite the working electrode and the reference electrode was a ring around the counter electrode. Both counter and reference electrodes were exposed to air. The fuel electrode compartment was sealed with a glass. Pt mesh was used as the current collector. Details of the cell configuration have been described previously [12].

The H_2 gas (BOC gases, 99.98%) was used directly from the gas bottle without being subjected to any additional drying (referred to as dry H_2). The water content of the dry H_2 used in the present study was estimated to be about 0.07% [12]. In moist H_2, H_2O was introduced into the H_2 gas through a bubbler system in a temperature-controlled bath resulting in 2% H_2O content in the gas stream. The flow rate of the hydrogen fuel was 100 ml min^{-1}. The P_{O_2} in dry H_2 (~0.07% H_2O) is typically 1.62×10^{-16} Pa and about 1.65×10^{-13} Pa for moist H_2 (2% H_2O) at 1000°C, as calculated from the observed open circuit potentials (OCP, which was about 1.280 V in dry H_2 and 1.080 V in moist H_2) [12].

The electrochemical impedance behaviour of anodes was studied with a Voltech, Model TF2000 frequency response analyser in conjunction with a potentiostat (Utah Electronics, Model 0152). The frequency range used was from 1 Hz to 100 kHz and the amplitude of the sinusoidal signal was 10 mV (peak-to-peak value). The impedance measurements were carried out under open circuit conditions and in the temperature range of 1000 to 800°C. The impedance data were analysed by a non-linear least square (CNLS) program developed by Macdonald [17,18].

The effect of H_2 concentration and P_{O_2} on the impedance behaviour of the H_2 oxidation reaction was studied in the H_2 concentration range from 98 to 10% at a constant 2% H_2O content in the gas. The H_2 concentration was changed by mixing it with N_2 as the balancing gas while maintaining a total flow at 100 ml min^{-1}. The P_{O_2} in the mixed gas was calculated from the open circuit potential according to the Nernst equation.

In separate experiments, impedance responses of a cell were studied while the anode (Ni or 80% Ni/20% Y-TZP cermet) was polarised with different current densities at 1000°C in 98% H_2/2% H_2O. The polarisation performance of anodes was also measured at 1000°C by a galvanostatic current interruption (GCI) technique in a current-generating mode (i.e., cell supplying current to an external load). The GCI technique used here has been described in detail elsewhere [19]. The morphology of the electrodes was examined by optical microscopy after investigation of the electrode kinetic behaviour.

3. Results and interpretation

Fig. 1 shows optical micrographs [(a)–(c)] of the polished cross-sections of Ni, 80% Ni/20% Y-TZP and 70% Ni/30% Y-TZP electrodes and a scanning electron micrograph (d) of a 70% Ni/30% Y-TZP cermet electrode after the cell evaluation. The thickness of the electrode coatings varied from ~25 μm for the Ni electrode to ~35 μm for the 70% Ni/30% Y-TZP cermet electrode. The size and distribution of Ni particles are clearly visible. Because the phase contrast between Ni and Y-TZP is so high, the

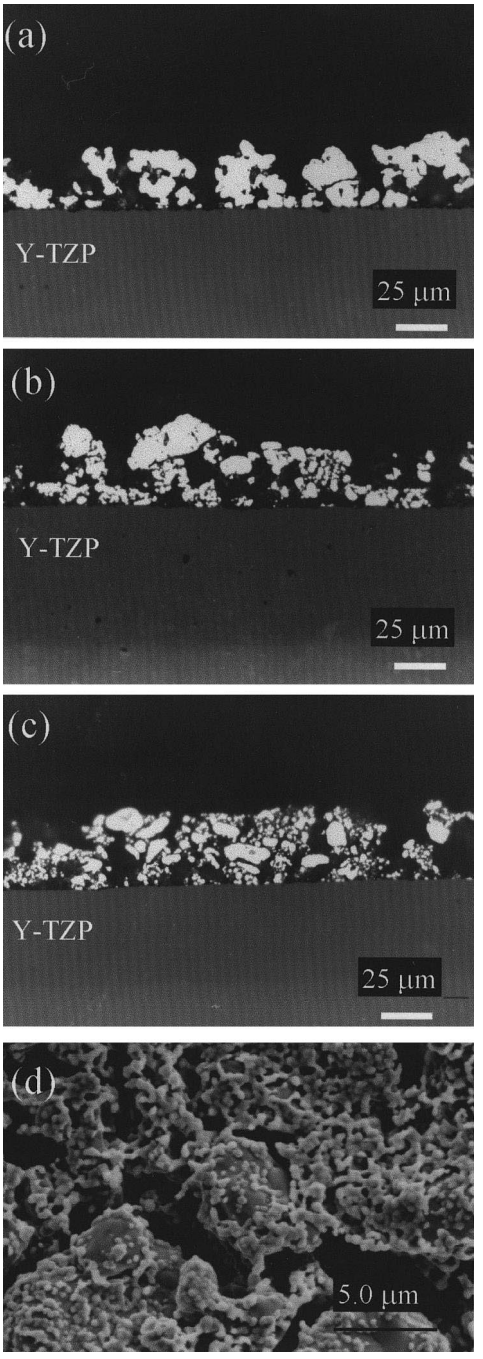

Fig. 1. Optical micrographs of polished cross-sections of (a) Ni, (b) 80% Ni/20% Y-TZP and (c) 70% Ni/30% Y-TZP cermet electrodes after fuel cell evaluation. (d) Scanning electron micrograph of a 70% Ni/30% Y-TZP cermet electrode.

Y-TZP particles cannot be seen clearly in these optical micrographs, however examination of these specimens with a scanning electron microscope showed that the size of the Y-TZP particles, distributed around the surface of Ni particles, was typically in the range of ~0.2 to 0.5 μm (Fig. 1d). The Ni electrode has a very open structure with large particles and pores (5 to 20 μm). For the 80% Ni/20% Y-TZP cermet electrode, the majority of Ni particles were in the range of 2 to 10 μm with a similar range for distribution of pores. Both Ni particles and pores were much smaller than those in Ni electrodes. As the Ni content decreased to 70 vol% in the cermet (70% Ni/30% Y-TZP electrode), the structure became more porous due to the increase of small Ni particles (1 to 5 μm size). The fine and porous structure of Ni/Y-TZP cermet electrodes as compared to the open and coarse structure of Ni electrodes indicates that the fine Y-TZP particles inhibit the growth and coarsening of Ni particles.

Fig. 2 shows polarisation curves for the H_2 oxidation reaction on Ni, 80% Ni/20% Y-TZP and 70% Ni/30% Y-TZP cermet electrodes in dry H_2 at 1000°C. The polarisation characteristics are essentially the same on Ni and Ni/Y-TZP electrodes. Three distinct polarisation regions were clearly observed as the current density increased. At low current densities (less than ~75 mA cm^{-2} – Region I), the overpotential losses (η) are strongly dependent on the current density and increase very rapidly with increasing current density. At intermediate current densities (Region II), the characteristics of η versus current density curves change significantly relative to Region I. In this region, η changes very little with increasing current density. However, at high current densities (Region III), η increases rapidly again with increasing current density. This behaviour may stem from the gas diffusion limitation. Most significantly, it is worth noting here that increasing the Y-TZP content in the cermet decreases the overall overpotential losses, similar to the effect of H_2O content in H_2 fuel on the reaction observed for Ni electrodes [12].

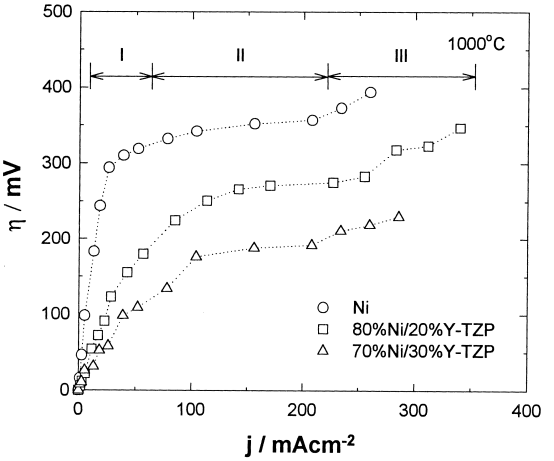

Fig. 2. Polarisation curves for H_2 oxidation for Ni and Ni/Y-TZP cermet electrodes, at 1000°C in dry H_2.

The effect of the Y-TZP phase in cermet electrodes on the polarisation behaviour is also clearly obvious from impedance results. Fig. 3 shows impedance spectra for Ni, 80% Ni/20% Y-TZP and 70% Ni/30% Y-TZP cermet electrodes in dry H_2 at 1000°C under open circuit conditions. The intercept of impedance spectra at high frequencies on the real impedance axis is the electrolyte resistance. The impedance curves are skewed and appear to consist of at least two overlapping semicircles, both depressed below the real axis. The impedance of Ni/Y-TZP cermet electrodes generally behaves very similarly to that of the Ni electrodes, except that the magnitude of the arcs (i.e., the electrode resistance, R) is much lower for the Ni/Y-TZP cermet electrodes. These observations are consistent with the lower overpotential losses observed for Ni/Y-TZP cermet electrodes compared to the Ni electrode (Fig. 2). The total electrode resistance was estimated by extrapolation of impedance arcs at low frequencies. In dry H_2, the total R value directly measured from

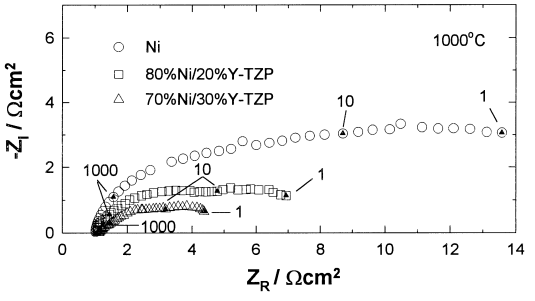

Fig. 3. Impedance spectra for H_2 oxidation for Ni and Ni/Y-TZP cermet electrodes at 1000°C in dry H_2 under open circuit conditions. Indicated numbers are frequencies in Hz.

low and high frequency intercepts is ~29 $\Omega\,cm^2$ for the Ni electrode, ~7 $\Omega\,cm^2$ for 80% Ni/20% Y-TZP and ~4 $\Omega\,cm^2$ for 70% Ni/30% Y-TZP cermet electrodes.

Fig. 4 shows impedance spectra (symbols) for H_2 oxidation for all three electrodes at 1000°C in moist H_2 (2% H_2O) under open circuit conditions. The solid lines in Fig. 4 are the fitted results of the CNLS program [17,18] and will be discussed in more detail later. The addition of 2% H_2O to the hydrogen gas has reduced the size of both the high and low frequency arcs, however the effect on the low frequency arc appears to be more dominant. In the case of Ni/Y-TZP cermet electrodes, both impedance arcs are clearly separated, indicating that the H_2 oxidation reaction on Ni/Y-TZP cermet electrodes is affected by at least two electrode processes in series [12]. For the Ni electrode, the process observed at high frequencies appears to dominate the reaction kinetics even though there is a substantial overlap of low and high frequency arcs. For Ni/Y-TZP cermet electrodes, the electrode process observed in the high frequency range became relatively less dominant with increasing Y-TZP content, as indicated by the relative change in the size of high and low frequency arcs (Fig. 4).

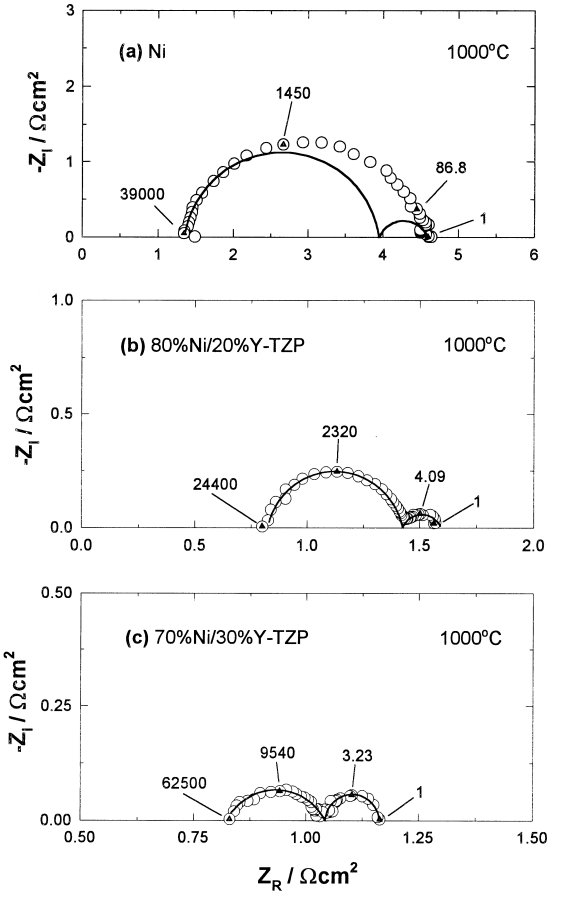

Fig. 4. Impedance spectra for H_2 oxidation for (a) Ni, (b) 80% Ni/20% Y-TZP and (c) 70% Ni/30% Y-TZP cermet electrodes at 1000°C in 98% H_2/2% H_2O under open circuit conditions. The symbols are the experimental data and solid lines are the fitted results by the CNLS program. Indicated numbers are frequencies in Hz.

In general, in solid electrode/electrolyte systems of the type studied here, the interface processes show a considerable frequency dispersion. Such behaviour is generally analysed by the inclusion of a constant phase element (CPE) in the equivalent circuit [13,20,21]. The CPE in parallel with a resistor leads to depressed semicircular arcs as observed in this work and often found for other solid electrolyte systems. The impedance of a CPE is represented by the following empirical equation [22]:

$$Z_{CPE} = A(j\omega)^{-n}, \tag{1}$$

where ω is the angular frequency and $j = \sqrt{-1}$. Both A and n may show temperature dependence. For $n = 0.5$, the CPE is a Warburg-type diffusion impedance. For $n = 1$, the CPE is a pure capacitance with $C = A^{-1}$, and for $n = -1$, the CPE is an inductance. The origin of CPE has not been fully understood. However, it has been shown that surface roughness may be an important contributing factor to the observed frequency dispersion [23] and CPE may be related to the fractal character of an electrode/electrolyte interface [24,25]. In any case CPE represents a distribution of time constants.

In this work it was found that the fitting of the experimental data to two Cole–Cole relaxation processes using the equivalent circuit shown in Fig. 5 by the CNLS program [17,18] is extremely good. Examples of fitting the CNLS program for the reaction on Ni and Ni/Y–TZP cermet electrodes at 1000°C in 98% H_2/2% H_2O are given as solid lines in Fig. 4. The results of the impedance parameters evaluated by the CNLS program are given in Table 1. In the table, α is a distribution parameter which

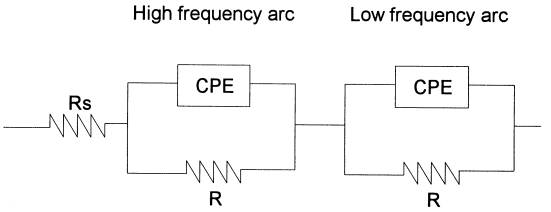

Fig. 5. An equivalent circuit consisting of two parallel combinations of electrode resistance, R, and a constant phase element (CPE), representing low and high frequency arcs. R_S is the ohmic resistance of the electrolyte.

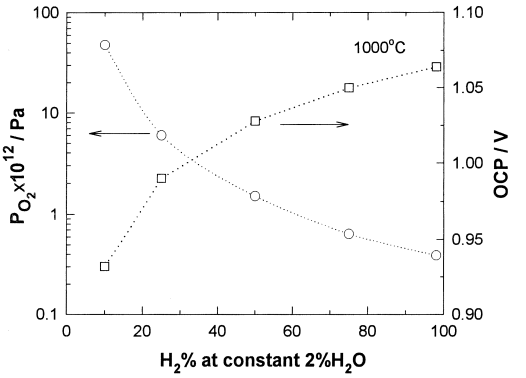

Fig. 6. Graphs showing change of P_{O_2} and OCP with H_2 concentration at a constant 2% H_2O, measured at 1000°C, for an 80% Ni/20% Y-TZP cermet electrode.

can be related to a more generalised CPE by $n = 1 - \alpha$ [26]. τ_0 is the time constant and R is the electrode resistance. In all cases, since the values of n ($= 1 - \alpha$) are above 0.7 and usually close to 1.0, an estimation of the capacitance has been made from the time constant ($\tau_0 = 1/\omega_0 = RC$, where ω_0 is the frequency at the apex of each arc). These capacitance values are also reported in Table 1. From the data in Table 1, it is obvious that the overall electrode resistance, the sum of low and high frequency components, decreases significantly with increasing additions of Y-TZP to Ni electrodes.

In the study of H_2 oxidation in the H_2/H_2O system, the H_2 concentration and oxygen partial pressure, P_{O_2}, are possibly the most important parameters influencing the kinetics of the reaction – the effect of H_2O content being closely related to that of P_{O_2} [12]. In the current work, for selected experiments, the H_2 concentration was changed by dilution with nitrogen gas at a constant water content (2% H_2O). As illustrated in Fig. 6 for an 80% Ni/20% Y-TZP cermet electrode, a decrease in the H_2 concentration (i.e., the H_2/H_2O ratio) leads to an increase in P_{O_2} (calculated from the OCP). Therefore, both the H_2 concentration and P_{O_2} change at the same time. Such experiments, although adding to the complexity, nevertheless can provide useful information about the reaction mechanism. Fig. 7 compares impedance spectra recorded at 1000°C, under open circuit conditions, for an 80% Ni/20% Y-TZP cermet electrode exposed to 98% and 10% H_2 concentration in the gas stream at a constant 2% H_2O content. On changing the H_2 concentration from 98 to 10%, the size of the low frequency arc increased, whereas the size of the high frequency arc decreased. In order to distinguish qualitatively the effect of H_2 concentration and P_{O_2} on the respective electrode processes, we plotted the electrode conductivity and capacitance for both high and low frequency arcs as a function of H_2 concentration (Fig. 8a) and P_{O_2} (Fig. 8b) for an 80% Ni/20% Y-TZP cermet electrode at 1000°C. In this diagram, σ_L and σ_H represent the electrode conductivity ($\sigma = 1/R$), and C_L and C_H represent the electrode capacitance of the low and high frequency arcs, respective-

Table 1
Parameters of Cole–Cole relaxation processes by the CNLS program at 1000°C in 98% H_2/2% H_2O

Electrode	Low frequency arc					High frequency arc				
	τ_0 (s)	R (Ω cm^2)	C (μF cm^{-2})	α	n ($1-\alpha$)	τ_0 (s)	R (Ω cm^2)	C (μF cm^{-2})	α	n ($1-\alpha$)
Ni	5.41×10^{-5}	0.65	8.35×10^{2}	0.24	0.76	1.23×10^{-4}	2.94	47	0.09	0.91
80% Ni/ 20% Y-TZP	3.42×10^{-2}	0.17	2.01×10^{5}	0.23	0.77	6.93×10^{-5}	0.60	116	0.12	0.88
70% Ni/ 30% Y-TZP	4.58×10^{-2}	0.12	3.72×10^{5}	0.02	0.98	1.96×10^{-5}	0.22	88	0.30	0.70

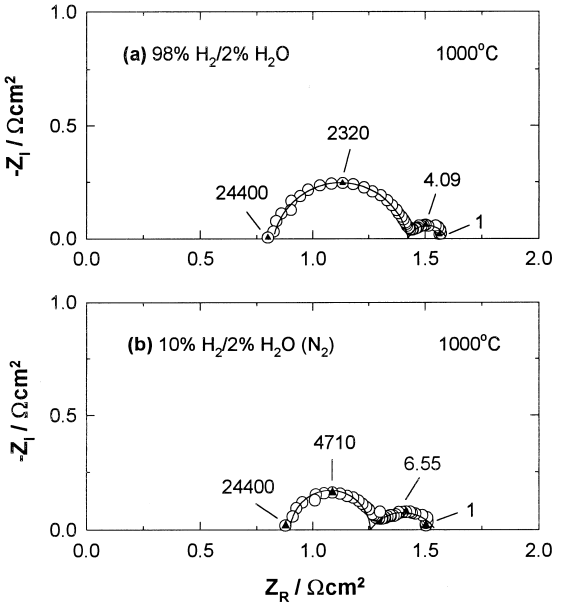

Fig. 7. Impedance spectra for H_2 oxidation on an 80% Ni/20% Y-TZP electrode, measured in 98% H_2 and 10% H_2 at a constant 2% H_2O at 1000°C under open circuit conditions. The symbols are the experimental data and lines are fitted results by the CNLS program. Indicated numbers are frequencies in Hz.

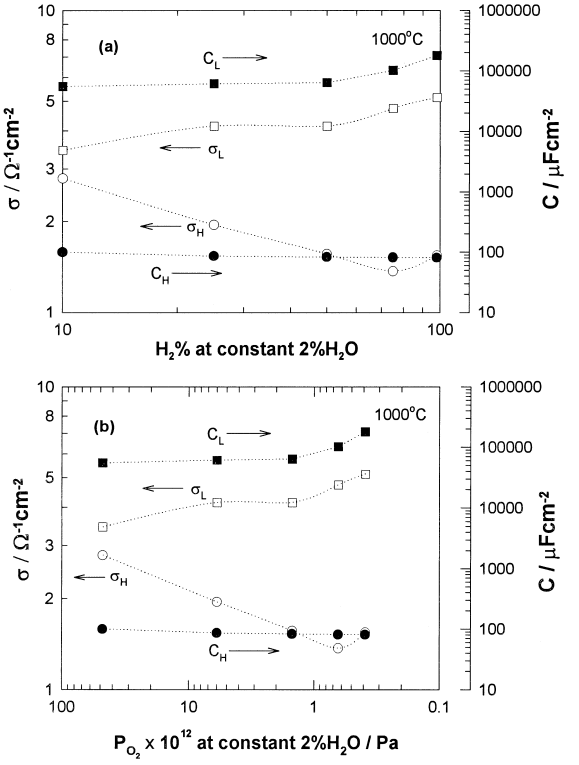

Fig. 8. Plots of electrode conductive and capacitive components of low and high frequency arcs versus: (a) H_2 concentration and (b) P_{O_2} for an 80% Ni/20% Y-TZP cermet electrode at a constant 2% H_2O, 1000°C. σ_H and σ_L – left axis. C_H and C_L – right axis.

ly. For the low frequency arc (represented by square symbols), both conductivity and capacitance, σ_L and C_L, increase with increasing H_2 concentration (despite a substantial decrease in P_{O_2}, Fig. 8a). This behaviour, where the reaction rate is enhanced by increasing the concentration of the reactant species, is common and is normally observed in similar electrochemical systems. However, the behaviour for the high frequency arc (represented by circular symbol) was significantly different. Although the capacitive component, C_H, changed very little with both H_2% and P_{O_2}, the electrode conductivity for the high frequency process, σ_H, increased with decreasing H_2 concentration or increasing P_{O_2} (H_2O/H_2 ratio) (Fig. 8b). Thus, the conductivity and capacitive components of the low and high frequency arcs behave differently as a function of P_{O_2} and the H_2 concentration. The reduction of σ_L values (or the reaction rate) with decreasing H_2 concentration, despite the two orders of magnitude increase in P_{O_2}, indicates that the low frequency electrode process is related to the H_2 concentration and to a less extent to P_{O_2} (H_2O/H_2 ratio). In contrast, the increase in the σ_H values (or the reaction rate) for the high frequency process with decreasing H_2 concentration or increasing P_{O_2} (H_2O/H_2 ratio) appears to indicate its dependence on P_{O_2} (H_2O/H_2 ratio). Similar behaviour was also observed for 70% Ni/30% Y-TZP cermet electrodes as shown in Fig. 9. For this electrode, the σ_L values for the low frequency process became smaller than that for the high frequency arc as the H_2 concentration decreased below 60%.

The effect of temperature in the 1000 to 800°C range on the high and low frequency impedance arcs is shown in Fig. 10 in the form of Arrhenius plots for the individual electrode conductivities (σ_H and σ_L) for 80% Ni/20% Y-TZP and 70% Ni/30% Y-TZP cermet electrodes in moist H_2 (2% H_2O) under open circuit conditions. For the Ni electrode, the total σ values are shown due to significant overlap of high

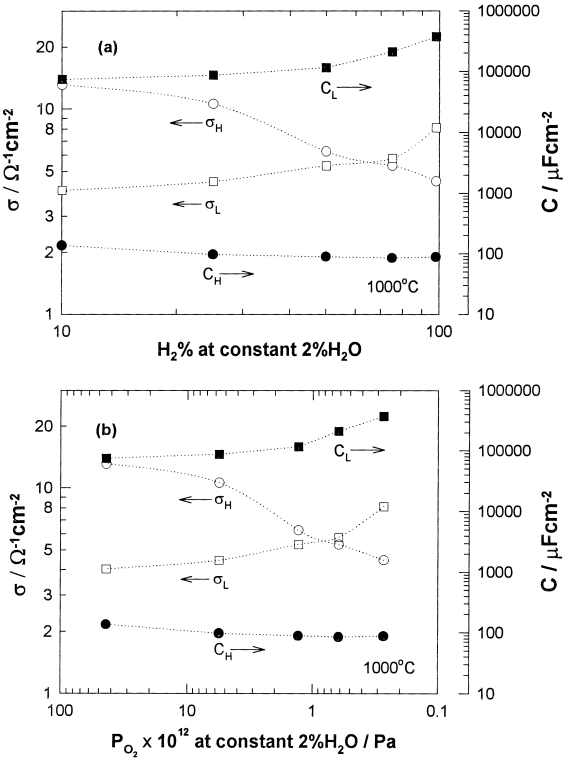

Fig. 9. Plots of electrode conductivity and capacitance of low and high frequency arcs (70% Ni/30% Y-TZP electrode, 2% H_2O, 1000°C) versus: (a) H_2 concentration and (b) P_{O_2}.

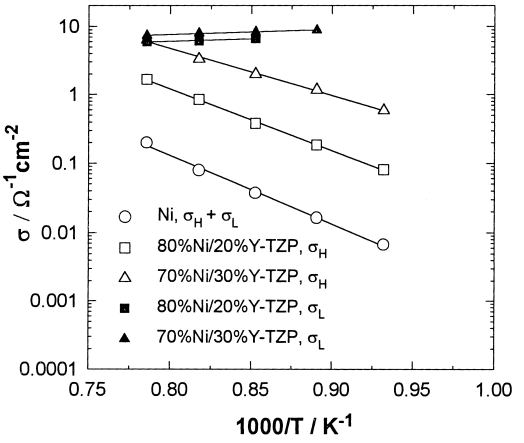

Fig. 10. Arrhenius plots of total σ for a Ni electrode and of individual conductivity of high and low frequency arcs, σ_H and σ_L, for Ni/Y-TZP cermet electrodes in 98% H_2/2% H_2O.

and low frequency arcs (see Fig. 4a). For σ_L, the activation energy, for cermet electrodes, is close to zero, indicating that the electrode process corresponding to the low frequency arc is essentially independent of temperature. However, the electrode process associated with the high frequency arc showed a strong dependence on temperature. On average, the activation energy for σ_H is 162±20 kJ mol^{-1} for cermet electrodes. A similar value was observed for the total ($\sigma_L + \sigma_H$) conductivity of the Ni electrode. On symmetric Ni/YSZ cermet electrode cells, Geyer et al. reported that the activation energy for the high frequency arc was about 100 kJ mol^{-1} while the low frequency arc was independent of temperature [27]. Okumura et al. have reported an activation energy of 125 kJ mol^{-1} for a 68% Ni/32% YSZ cermet electrode [28]. For a screen-printed Ni/Y_2O_3–ZrO_2 cermet electrode, an activation energy of ~145 kJ mol^{-1} was evaluated from the electrode conductivity in the temperature range 750 to 950°C by Divisek et al. [29].

Fig. 11 shows the electrode resistance, R, measured by impedance spectroscopy while the anode was polarised with different overpotentials (current densities) in 98% H_2/2% H_2O at 1000°C. In Fig. 11a, the electrode resistance for high and low frequency arcs, R_H and R_L, has been plotted as a function of the overpotential for the 80% Ni/20% Y-TZP cermet electrode. R_H decreased with increasing overpotential. In contrast, R_L was almost independent of overpotential. Similar behaviour was observed for the 70% Ni/30% Y-TZP cermet electrode. Since it is only the high frequency arc which is mainly affected by the overpotential, in Fig. 11b the total electrode resistance for Ni and 80% Ni/20% Y-TZP cermet electrodes has been compared as a function of overpotential to demonstrate the rapid reduction in the electrode resistant with overpotential for the Ni electrode. The reduction of the electrode resistance for a Ni/YSZ cermet electrode as a function of current passing through the cell has also been reported by van Herle et al. [30].

For the overall electrode reaction kinetics, the ratio of σ_H/σ_L can be used as an indicator for the dominant roles of processes associated with the low or the high frequency arcs. For $\sigma_H/\sigma_L \gg 1$ the low frequency process, and for $\sigma_H/\sigma_L \ll 1$ the high frequency process, will control the reaction kinetics.

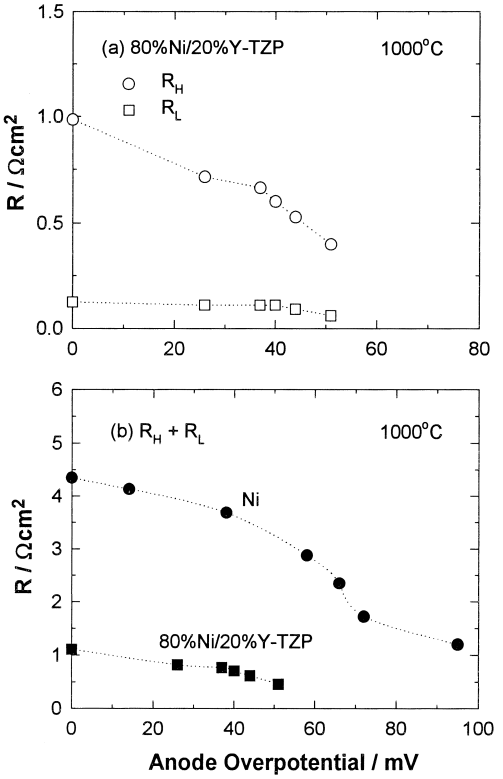

Fig. 11. Plots of electrode resistance as a function of anode overpotential at 1000°C in 98% H_2/2% H_2O: (a) electrode resistance of high and low frequency arcs, R_H and R_L, for an 80% Ni/20% Y-TZP cermet electrode and (b) total electrode resistance for Ni and 80% Ni/20% Y-TZP electrodes.

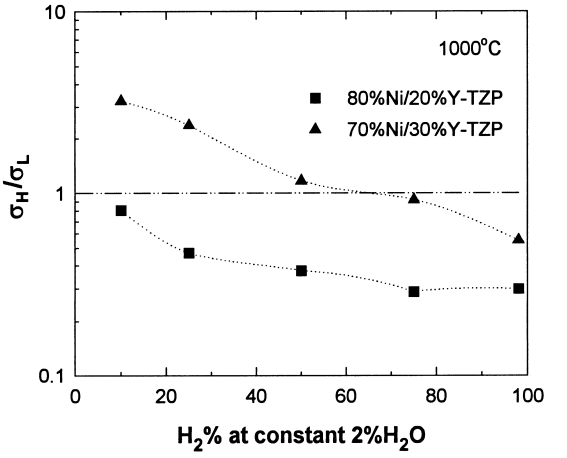

Fig. 12. Plots of σ_H/σ_L ratio against H_2 concentration on 80% Ni/20% Y-TZP and 70% Ni/30% Y-TZP cermet electrodes, measured at 1000°C under open circuit conditions.

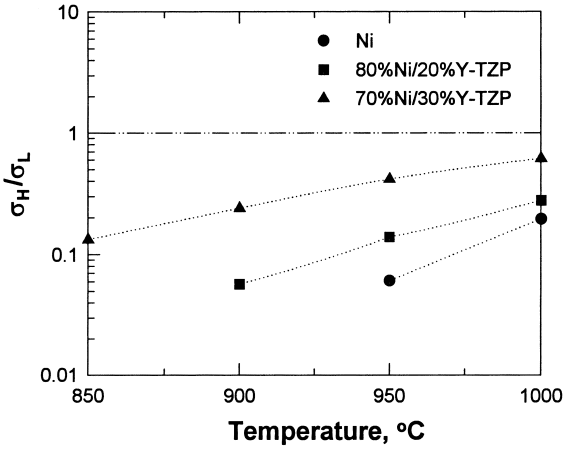

Fig. 13. Plots of σ_H/σ_L ratio versus temperature for Ni, 80% Ni/20% Y-TZP and 70% Ni/30% Y-TZP cermet electrodes, measured in 98% H_2/2% H_2O under open circuit conditions.

Fig. 12 shows the σ_H/σ_L ratio at 1000°C as a function of H_2 concentration for 80% Ni/20% Y-TZP and 70% Ni/30% Y-TZP cermet electrodes for constant 2% H_2O content in the gas under open circuit conditions. Qualitatively, the electrode process in the low frequency range becomes increasingly important with decreasing H_2 concentration and with increasing Y-TZP content in the Ni cermet electrode. In the case of a 70% Ni/30% Y-TZP cermet electrode, the σ_H/σ_L ratio became greater than 1 when the H_2 concentration decreased below 60%, indicating that the reaction kinetics is becoming more dominated by the slower process. Fig. 13 compares the σ_H/σ_L ratio at different temperatures for Ni and Ni/Y-TZP cermet electrodes in 98% H_2/2% H_2O under open circuit conditions. Because of the very different activation energies associated with both processes, the electrode process associated with high frequency (with high activation energy) becomes relatively more significant with decreasing temperature, while the electrode process observed at low frequencies (with little temperature dependence) becomes increasingly less dominant as the temperature decreases.

4. Discussion

The significant observations of this work can be summarised as follows:

- The polarisation curves for all electrodes studied showed three distinct regions as a function of the current density. In Region I (low current densities), η showed a strong dependence on the current density, in Region II (intermediate current densities) there was little increase of η with increasing current densities, and in Region III (high current densities) η increased rapidly with the current density. This behaviour is consistent with that observed before for the Ni electrode on Y-TZP electrolyte [12].
- The addition of Y-TZP to Ni electrodes led to a substantial reduction in η. The impedance characteristics for the H_2 oxidation reaction on Ni and Ni/Y-TZP cermet electrodes were similar in both dry and moist H_2 (2% H_2O) except that the addition of Y-TZP to the Ni electrodes significantly reduced the size of both low and high frequency arcs. This behaviour was similar to that observed for Ni electrodes when water was added to dry hydrogen [12].
- The impedance behaviour for the H_2 oxidation reaction in moist H_2 for 80% Ni/20% Y-TZP and 70% Ni/30% Y-TZP cermet electrodes was characterised by two clearly separated arcs. Both conductivity and capacitive components of the low frequency arc (σ_L and C_L) decreased with decreasing H_2 concentration. C_L was in the range of $\sim 10^3$ μF cm^{-2} for the Ni electrode and $\sim 10^5$ μF cm^{-2} for Ni/Y-TZP cermet electrodes, about two orders of magnitude difference. The conductivity and capacitive components of the high frequency arc (σ_H and C_H) behaved very differently. σ_H increased with decreasing H_2 concentration and C_H appears to be independent of H_2 concentration and P_{O_2}. The increase in σ_H is more likely to be related to P_{O_2} (H_2O/H_2 ratio) as both P_{O_2} and the H_2O/H_2 ratio increased significantly at the same time as the H_2 concentration decreased. C_H was ~ 50 μF cm^{-2} for the Ni electrode and ~ 100 μF cm^{-2} for Ni/Y–TZP cermet electrodes.
- The addition of water to dry hydrogen reduced both high and low frequency arcs for all three electrodes. The effect was more pronounced for the low frequency arc.
- The activation processes associated with low and high frequency arcs are very different. The low frequency arc was almost independent of temperature, whereas the process associated with the high frequency arc showed a strong temperature dependence (activation energy: 162 ± 20 kJ mol^{-1}).
- On polarisation of cermet electrodes with a potential, the electrode resistance associated with the high frequency arc decreased with increasing polarisation potential while the effect on the low frequency arc was relatively small.
- The impedance behaviour for H_2 oxidation on the Ni electrode was dominated by the high frequency arc and the effect of polarisation potential in reducing the electrode resistance was more significant compared to that for Ni/Y–TZP cermet electrodes.

The observation of two clearly separated arcs in the frequency domain indicates that H_2 oxidation at Ni/Y-TZP cermet electrodes is controlled by at least two electrode processes in series, similar to the behaviour observed previously for Ni electrodes [12]. More importantly, these two arcs show very different behaviour with respect to temperature, H_2 concentration, P_{O_2} (H_2O/H_2 ratio) and the polarisation potential.

4.1. Electrode process corresponding to the low frequency arc in moist H_2

The reports in the literature on the role of water content in H_2 and the H_2 concentration have widely varying conclusions. Geyer et al. [27], in an investigation of H_2 oxidation on a symmetrical Ni/YSZ cermet electrode cell by impedance spectroscopy, in undiluted H_2 between 800 and 1000°C, have reported that σ_L is independent of temperature and the electrode conductivity corresponding to the low frequency arc increased very rapidly with increasing H_2O content (up to ~20%), consistent with observations of the present study. These authors have attributed the low frequency arc to a gas diffusion

process along the channels of the interconnect. Mogensen and Lindegaard [13] studied the impedance behaviour of H_2 oxidation at Ni/YSZ cermet electrodes at constant H_2 concentration and oxygen partial pressure (P_{O_2}) by keeping OCP constant at 1000°C. Their results showed that, at a constant P_{O_2}, both conductive and capacitive components of the low frequency arc decrease much more rapidly with decreasing H_2 concentration than that observed in the present study. However, in the present work, a decrease in the H_2 concentration also led to an increase in P_{O_2} (H_2O/H_2 ratio). Mogensen and Lindegaard [13] have also reported that, at a constant H_2 concentration, both conductive and capacitive components of the low frequency arc increase with increasing H_2O content (or increasing P_{O_2}) in the range 0.22 to 3% H_2O. Their observations are consistent with ours and confirm that the P_{O_2} (H_2O/H_2 ratio) plays an active role in promoting the hydrogen adsorption/diffusion processes at the Ni surface. Primdahl and Mogensen [31], in an impedance study of the H_2 oxidation reaction on Ni/YSZ cermet electrodes over a wide range of H_2 concentration and H_2O content, have reported three impedance arcs for the electrode behaviour. The low and medium frequency arcs were essentially independent of temperature, similar to the behaviour observed for the low frequency arc in the present study. However, the electrode resistance associated with the low and medium frequency arcs decreased with increasing polarisation potential, in contradiction to the observations of this study.

In the present study, the characteristics of the electrode conductive and capacitive components of the low frequency arc (very large time constant, no effect of temperature and the dependence on hydrogen concentration) appear to indicate that the electrode process is associated with a hydrogen dissociative adsorption or a diffusion step on the Ni surface (see discussion below). Furthermore, the polarisation potential has no effect on σ_L, indicating that the hydrogen adsorption or the diffusion processes may not involve a charged species such as H^+.

Usually in electrode kinetic studies for solid electrolyte systems, processes such as adsorption/dissociation or diffusion are slow and are observed at low frequencies. The charge transfer process in general is faster and is observed at high frequencies consistent with the proposed mechanism [12]. Also, the hydrogen dissociative adsorption or diffusion processes are known to have low activation energy. For example, Mulins et al. have measured surface diffusion and activation of hydrogen and deuterium on a Ni (100) surface by the laser induced desorption method between 211 and 263 K and reported an activation energy of 14.6 kJ mol^{-1} [32]. Gomer reported activation energies of 272 and 125 kJ mol^{-1} for CO and oxygen surface diffusion, respectively, on a W boundary free surface [33]. On the same surface, the activation energy for hydrogen surface diffusion was 40–67 kJ mol^{-1}. The relatively low activation energy for hydrogen surface diffusion may be related to the small size of the hydrogen atom and the small number of formal bonds made with the surface.

Furthermore, the observation (reduction of the size of the low frequency arc with the addition of H_2O content [12,14,34] for all three electrodes or the addition of Y-TZP to Ni electrodes) supports the view that the low frequency arc is associated with an adsorption or a diffusion process of hydrogen species on the Ni surface rather than a pure hydrogen gas phase diffusion. In dry hydrogen (low P_{O_2}) with very little moisture, the low frequency arc dominates the reaction kinetics. With the addition of 2% H_2O to H_2, the magnitude of this arc decreases substantially. This behaviour for the Ni electrodes was explained in a previous publication [12] where the increase in the H_2O content in H_2 increased the concentration of O_{ads} sites or led to the formation of sub-surface oxide sites on the Ni surface. The presence of O_{ads} sites or the formation of sub-oxide sites enhance the hydrogen adsorption/dissociation and hydrogen diffusion processes on the Ni metal surface through the spillover mechanism [12,35]. According to Curtis-Conner et al. [36], spillover enhances the kinetics of adsorption processes, whereas Robell et al. [37] and Kramer et al. [38] studied the kinetics of spillover hydrogen species on platinised carbon and platinised alumina, respectively, and concluded that the rate of spillover is limited by the surface diffusion. In dry hydrogen, the concentration of active sites (i.e. O_{ads} or a Ni–O suboxide) is very low for hydrogen adsorption or diffusion of hydrogen species to proceed at a reasonable rate. The addition of H_2O (e.g., 2% H_2O) leads to a significant increase in P_{O_2}

in the H_2 fuel (from $\sim 10^{-16}$ Pa in dry H_2 to $\sim 10^{-13}$ Pa in 98% H_2/2% H_2O) and a consequential increase in the concentration of active O_{ads} or Ni–O suboxide sites at the Ni surface. This would lead to a significant reduction of the overall electrode resistance, as is indeed indicated by the dramatic reduction of the size of the impedance arcs, in particular the low frequency arc, for Ni and Ni/Y-TZP electrodes. This mechanism is further supported by the observation that the addition of Y-TZP to Ni had a somewhat similar effect as the water content (increase in P_{O_2}) in promoting adsorption/diffusion of hydrogen on the Ni surface through a spillover mechanism by providing active O_{ads} or $O–S_{Ni}$ sites on or next to the Ni surface. However, quantitatively how the addition of Y-TZP to Ni and the water content in the fuel influence the reaction kinetics will very much depend on the electrode microstructure.

From the bulk of observations of this study and the evidence presented above, the low frequency arc appears most likely to be associated with a slow hydrogen dissociative adsorption or a surface diffusion process at the Ni surface.

4.2. Electrode processes corresponding to the high frequency arc in moist H_2

The second electrode process associated with the high frequency arc had a high activation energy, small time constant, strong dependence on P_{O_2} (H_2O/H_2 ratio) and a complex relationship with respect to H_2 concentration. The capacitive component associated with the high frequency arc, C_H, is much smaller, independent of both H_2 concentration and P_{O_2}, and behaves more or less like a double layer capacitance as expected for a metal/solid electrolyte interface [39], thus indicating that the process associated with this arc is taking place close to the electrode/electrolyte interface region. Based on the available evidence, this process appears to be related to a charge transfer reaction at the electrode/electrolyte interface. This assertion is also supported by the fact that the polarisation resistance decreased substantially for the high frequency arc with increasing polarisation potential, indicating that, quite likely, a charged specie is involved in the rate limiting process. Moreover, such behaviour is typical of the charge transfer limiting process. Furthermore, the strong temperature dependence for this arc (the high activation energy of ~ 162 kJ mol^{-1}) for Ni and Ni/Y-TZP cermet electrodes cannot be explained by the gaseous or surface diffusion of hydrogen. Also, there is no evidence from the present studies to indicate that the reaction is limited by the diffusion of H_2O product near the electrode/electrolyte interface as suggested by others [40,41].

In a previous publication, the charge transfer process was split into the following steps [12]:

$$H_{ads}–S_{Ni} \text{ and/or } H_{ads}–O–S_{Ni} \rightarrow H_{ads,\ Y\text{-}TZP} \text{ (TPB)}, \tag{2a}$$

$$O^{2-}_{Y\text{-}TZP} + 2H_{ads,\ Y\text{-}TZP} \rightarrow H_2O + 2e_{Y\text{-}TZP} \text{ (near TPB)} + V_{\ddot{O},\ Y\text{-}TZP}, \tag{2b}$$

$$2e_{Y\text{-}TZP} \rightarrow 2e_{Ni}, \tag{2c}$$

where $O^{2-}_{Y\text{-}TZP}$ is an oxygen on a lattice site, $V_{\ddot{O},\ Y\text{-}TZP}$ is an oxygen vacancy on the Y-TZP surface, S_{Ni} is an active site on the Ni surface and $O–S_{Ni}$ is an active site on the Ni surface adjacent to an O_{ads} and/or sub-NiO. From the proposed reaction steps, the overall reaction rate for this electrode process is determined by the transfer of hydrogen species from Ni to the zirconia surface (step (2a)) and the charge transfer on the zirconia electrolyte surface (steps (2b) and (2c)). Step (2b) would be facilitated by the high oxygen-ion conductivity of the electrolyte and step (2c) would be enhanced by high surface electronic conductivity of the electrolyte phase. The evidence for this has been provided by Uchida et al. [42] and Jiang and Badwal [12]. Uchida et al. found that polarisation losses for the H_2 oxidation reaction for Pt electrodes decreased with an increase in the oxygen-ion conductivity of zirconia electrolytes, whereas Jiang and Badwal demonstrated that enhancing the electronic conductivity of the Y-TZP electrolyte surface, by doping with electronically conducting oxides, mainly increased the electrode conductivity of the high frequency arc.

Several authors have reported the dependence of electrode resistance on hydrogen and water content in the fuel gas, however there is no consistent behaviour, indicating that the electrode preparation

(microstructure) may play an important role. In the present study, the complex influence of H_2 concentration and P_{O_2} (H_2O/H_2 ratio) on the reaction kinetics is possibly indicated by the observation that the electrode conductivity for the high frequency process (σ_H) initially decreased with decreasing H_2 concentration with a minimum at ~75% H_2. However, the σ_H values increased when the H_2 concentration was lower than ~75% for an 80% Ni/20% Y-TZP cermet electrode (see Fig. 8). The initial decrease of σ_H with H_2 concentration is understandable from the viewpoint of the reduced concentration of H_2 reactant in the electrode/electrolyte interface region. However, the subsequent increase of σ_H with decreasing hydrogen concentration is somewhat more difficult to explain. In the experiments performed in the present study to demonstrate the dependence of high and low frequency arcs on the hydrogen concentration, the P_{O_2} in the gas stream increased from 3×10^{-13} Pa to 5×10^{-11} Pa and the H_2O/H_2 ratio increased from 0.0204 to 0.2 as the H_2 content in the fuel gas was diluted from 98 to 10% at constant 2% H_2O. Therefore, it is possible that an increase in the σ_H value with decreasing hydrogen concentration is more tied to the significant increase in P_{O_2} (H_2O/H_2 ratio).

Mizusaki et al. [10] studied the H_2 oxidation reaction on Ni patterned electrodes at 700°C and their impedance results showed that, at a H_2O content of ~1.7%, the electrode conductivity (only one impedance arc was observed but the behaviour was similar to that of the high frequency arc) is essentially independent of H_2 concentration. However, at a lower H_2O content ($\leq$0.85%), the electrode conductivity showed a slight decrease with decreasing H_2 concentration. At a constant H_2 concentration (~1 to 10% H_2), the electrode conductivity was proportional to the H_2O content. On a point Ni electrode, Mohamedi-Boulenouar et al. [34] reported a reaction order of 0.5 with respect to the H_2O content at a constant H_2 concentration of 70%. On Ni/YSZ cermet electrodes Mogensen et al. [13,31] observed that the decrease in σ_H with decreasing H_2 concentration at constant P_{O_2} or with decreasing H_2O content at constant H_2 is much smaller than that for the electrode conductivities of both low and medium frequency arcs. Also, on Ni/YSZ cermet electrodes, Geyer et al. [27] reported a significant increase of σ_H with increasing H_2O content in undiluted H_2. Thus, in general, it appears that in moist H_2, P_{O_2} (H_2O/H_2 ratio) play a more dominant role in the electrode process associated with the high frequency arc. It is possible that, near the interface region, the oxygen species from the dissociation of water may contribute to the process of hydrogen diffusion from the Ni surface to the Y-TZP surface near the interface region (step (2a)) possibly by bridging these two surfaces through adsorbed oxygen species, O_{ads} or a suboxide.

4.3. The role of Y-TZP in Ni cermet electrodes and water content in the fuel gas

The particle size, ratio and the distribution of zirconia and Ni are very critical to the performance of Ni/zirconia cermet electrodes as demonstrated by numerous groups [3,4,43]. The much lower electrode resistance of Ni/Y-TZP cermet electrodes clearly demonstrates that the Y-TZP in the cermet electrodes significantly increases the active reaction area. The magnitude of both high and low frequency impedance arcs decreases as the Y-TZP content in Ni cermet electrodes increases. In order to discuss the role of Y-TZP in Ni cermet electrodes, two aspects which need to be considered are: the effect of Y-TZP in modifying the electrode microstructure and secondly how the presence of Y-TZP next to Ni particles changes the kinetics of the H_2 oxidation reaction.

The effect of the addition of Y-TZP in Ni electrodes on the electrode microstructure can be clearly seen from the optical micrographs (Fig. 1) and SEM examination of Ni and Ni/Y–TZP electrodes. With increasing zirconia content, the Ni particle size decreases substantially with a much finer distribution of pores. This behaviour occurs mainly due to the inhibiting effect of fine Y-TZP particles on the coarsening and growth of Ni particles. The addition of Y-TZP also increases the electrode/electrolyte interface contact area as clearly indicated by an increase in C_H from ~50 μF cm^{-2} for Ni electrodes to ~100 μF cm^{-2} for Ni/Y-TZP cermet electrodes. Other authors, for Ni/YSZ cermet electrodes with YSZ content around 50 to 60%, have reported C_H values in the range 200 to 700 μF cm^{-2} [31].

The effect of Y-TZP in Ni cermet electrodes on

the kinetics of the H_2 oxidation reaction is clearly obvious from the observed polarisation behaviour. The higher the Y-TZP content, the lower the overpotential losses. Most interestingly, the effect of Y-TZP addition was similar to that of H_2O content on the polarisation curves observed for Ni electrodes as the H_2O content in H_2 increased [12]. This indicates that Y-TZP particles in the cermet have a similar effect as the H_2O/H_2 ratio in promoting dissociation/diffusion of hydrogen on the Ni surface through a spillover mechanism by providing active O_{ads} or $O–S_{Ni}$ sites on or next to the Ni surface. The enhancement effect is also indicated by the substantial increase in C_L from $\sim 10^3$ μF cm^{-2} for the Ni electrode to $\sim 10^5$ μF cm^{-2} for Ni/Y–TZP cermet electrodes, measured at 1000°C in 98% H_2/2% H_2O. Nevertheless, from the observation in this study, it is clear that a change in the microstructure of Ni/Y-TZP cermet electrodes has no effect on the reaction mechanism for H_2 oxidation, as evident from the similar impedance and polarisation behaviour of Ni and Ni/Y-TZP electrodes.

As discussed above, the low frequency arc is associated with the dissociation adsorption or surface diffusion process and the high frequency arc is associated with the charge transfer (activation) polarisation. Therefore, the effect of Y-TZP in the Ni cermet electrode on the reaction kinetics could be measured by the relative change in the σ_H and σ_L values as shown in Figs 12 and 13. Qualitatively, the hydrogen adsorption or surface diffusion process becomes increasingly important with decreasing H_2 concentration and with increasing Y-TZP content in the Ni cermet electrode (complexity of the electrode microstructure) (Fig. 12). However, due to the very different activation energy for hydrogen surface dissociation/diffusion and the charge transfer steps, the activation polarisation becomes increasingly dominant as the temperature decreases and as the Y-TZP content in the Ni cermet electrode decreases (Fig. 13).

5. Conclusions

In moist H_2, the impedance behaviour for the H_2 oxidation reaction on Ni/Y-TZP cermet electrodes is characterised by two well-separated frequency arcs, indicating that the H_2 oxidation reaction on Ni and Ni/Y-TZP cermet electrodes is controlled by at least two rate limiting processes in series. The electrode processes associated with the low and high frequency arcs behave very differently with respect to the H_2 concentration, P_{O_2} (H_2O/H_2 ratio), the temperature and the polarisation potential. The electrode process at the low frequency arc has been identified as the hydrogen dissociation/diffusion process on the Ni surface (the first electrode process), and that at the high frequency arc as the hydrogen transfer from Ni to the Y-TZP surface followed by charge transfer steps on the Y-TZP electrolyte surface near the TPB region (the second electrode process). The Y-TZP phase in the Ni cermet electrodes has no effect on the reaction mechanism but plays an important role in modifying the electrode microstructure and the reaction kinetics. The effect of Y-TZP in the Ni cermet electrodes on the reaction kinetics can be qualitatively measured by the change in the σ_H/σ_L ratio. There is clear shifting of the rate determining step of the H_2 oxidation reaction from a dominant activation polarisation for Ni electrodes to a mixed process of activation and adsorption or surface diffusion for Ni/Y-TZP cermet electrodes.

Acknowledgements

Technical help from Kylie Crane for the preparation of Ni and Ni/Y-TZP cermet electrodes and Y-TZP electrolyte disks is greatly appreciated. We would also like to thank Dr J. Drennan for the optical micrographs and Dr S. Amarasinghe and Fabio Ciacchi for reviewing this paper.

References

[1] N.Q. Minh, T. Takahashi, Science and Technology of Ceramic Fuel Cells, Elsevier, Amsterdam, 1995.
[2] D.W. Dees, T.D. Claar, T.E. Easler, D.C. Fee, F.C. Mrazek, J. Electrochem. Soc. 134 (1987) 2141.
[3] T. Kawada, N. Sakai, H. Yokokawa, M. Dokiya, J. Electrochem. Soc. 137 (1990) 3042.

[4] S. Murakami, Y. Akiyama, N. Ishida, T. Yasuo, T. Saito, N. Furukawa, in: F. Grosz, P. Zegers, S.C. Singhal, O. Yamamoto (Eds.), Proceedings of the 2nd International Symposium on Solid Oxide Fuel Cells, Commission of the European Communities, Luxembourg, 1991, p. 561.
[5] M. Watanabe, H. Uchida, H. Suzuki, A. Tsuno, in: M. Dokiya, O. Yamamoto, H. Tagawa, S.C. Singhal (Eds.), Proceedings of the 4th International Symposium on Solid Oxide Fuel Cells, The Electrochemical Society Proceedings Series, The Electrochemical Society, Pennington, NJ, 1995, p. 750.
[6] T. Setoguchi, K. Okamoto, K. Eguchi, H. Arai, J. Electrochem. Soc. 139 (1992) 2875.
[7] P.K. Srivastava, T. Quach, Y.Y. Duan, R. Donelson, S.P. Jiang, F.T. Ciacchi, S.P.S. Badwal, Solid State Ionics 99 (1997) 311.
[8] E. Ivers-Tiffee, W. Lohwasser, R. Manner, G. Preu, W. Wersing, in: M. Dokiya, O. Yamamoto, H. Tagawa, S.C. Singhal (Eds.), Proceedings of the 4th International Symposium on Solid Oxide Fuel Cells, The Electrochemical Society Proceedings Series, The Electrochemical Society, Pennington, NJ, 1995, p. 1039.
[9] T. Norby, O.J. Velle, H. Leth-Olsen, R. Tunold, in: S.C. Singhal, H. Iwahara (Eds.), Proceedings of the 3rd International Symposium on Solid Oxide Fuel Cells, The Electrochemical Society Proceedings Series, The Electrochemical Society, Pennington, NJ, 1993, p. 473.
[10] J. Muzusaki, H. Tagawa, T. Saito, T. Yamamura, K. Kamitani, K. Hirano, S. Ehara, T. Takagi, T. Hikita, M. Ippommatsu, S. Nakagawa, K. Hashimoto, Solid State Ionics 70/71 (1994) 52.
[11] S.P. Jiang, in: S.P.S. Badwal, M.J. Bannister, R.H.J. Hannink (Eds.), Science and Technology of Zirconia, Vol. V, Technomic Publishing Co, Lancaster, 1993, p. 819.
[12] S.P. Jiang, S.P.S. Badwal, J. Electrochem. Soc. 144 (1997) 3777.
[13] M. Mogensen, T. Lindegaard, in: S.C. Singhal, H. Iwahara (Eds.), Proceedings of the 3rd International Symposium on Solid Oxide Fuel Cells, The Electrochemical Society Proceedings Series, The Electrochemical Society, Pennington, NJ, 1993, p. 484.
[14] D.W. Dees, U. Balachandran, S.E. Dorris, J.J. Heiberger, C.C. McPheeters, J.J. Picciolo, in: S.C. Singhal (Ed.), Proceedings of the 1st International Symposium on Solid Oxide Fuel Cells, The Electrochemical Society Proceedings Series, The Electrochemical Society, Pennington, NJ, 1989, p. 317.
[15] M. Mogensen, S. Skaarup, Solid State Ionics 86–88 (1996) 1151.
[16] M. Mogensen, in: F.W. Poulsen, J.J. Bentzen, T. Jacobsen, E. Skou, M.J.L. Ostergard (Eds.), High Temperature Electrochemical Behaviour of Fast Ion and Mixed Conductors, Publisher, Riso, Denmark, 1993, p. 117.
[17] J.R. MacDonald, Impedance Spectroscopy – Emphasising Solid Materials and Systems, Wiley-Interscience, New York, 1987.
[18] J.R. MacDonald, J. Electroanal. Chem. 223 (1987) 25.
[19] S.P.S. Badwal, N. Nardella, Solid State Ionics 40/41 (1990) 878.
[20] J.F. McCann, S.P.S. Badwal, J. Electrochem. Soc. 129 (1982) 551.
[21] S. Elangovan, A. Khandkar, M. Liu, M. Timper, in: D.D. Macdonald, A.C. Khandkar (Eds.), Proceedings of the Symposium on High Temperature Electrode Materials and Characterization, The Electrochemical Society Proceedings Series, The Electrochemical Society, Pennington, NJ, 1991, p. 191.
[22] K.S. Cole, J. Cole, Chem. Phys. 9 (1941) 341.
[23] W. Scheider, J. Phys. Chem. 79 (1975) 127.
[24] A. Le Mehaute, G. Crepy, Solid State Ionics 9/10 (1983) 17.
[25] S.H. Liu, Phys. Rev. Lett. 55 (1985) 529.
[26] J.R. MacDonald, Solid State Ionics 13 (1984) 147.
[27] J. Geyer, H. Kohlmuler, H. Landes, R. Stubner, in: U. Stimming, S.C. Singhal, H. Tagawa, W. Lehnert (Eds.), Proceedings of the 5th International Symposium on Solid Oxide Fuel Cells, The Electrochemical Society Proceedings Series, The Electrochemical Society, Pennington, NJ, 1997, p. 585.
[28] K. Okumura, Y. Yamamoto, T. Fukui, S. Hanyu, Y. Kubo, Y. Esaki, M. Hattori, A. Kusunoki, S. Takeuchi, in: S.C. Singhal, H. Iwahara (Eds.), Proceedings of the 3rd International Symposium on Solid Oxide Fuel Cells, The Electrochemical Society Proceedings Series, The Electrochemical Society, Pennington, NJ, 1993, p. 444.
[29] J. Divisek, A. Kornyshev, W. Lehnert, U. Stimming, I.C. Vinke, K. Wippermann, in: U. Stimming, S.C. Singhal, H. Tagawa, W. Lehnert (Eds.), Proceedings of the 5th International Symposium on Solid Oxide Fuel Cells, The Electrochemical Society Proceedings Series, The Electrochemical Society, Pennington, NJ, 1997, p. 606.
[30] J. van Herle, R. Ihringer, A.J. McEvoy, in: U. Stimming, S.C. Singhal, H. Tagawa, W. Lehnert (Eds.), Proceedings of the 5th International Symposium on Solid Oxide Fuel Cells, The Electrochemical Society Proceedings Series, The Electrochemical Society, Pennington, NJ, 1997, p. 565.
[31] S. Primdahl, M. Mogensen, J. Electrochem. Soc. 144 (1997) 3409.
[32] D.R. Mullin, B. Roop, S.A. Costello, J.M. White, Surf. Sci. 186 (1987) 67.
[33] R. Gomer, in: Field Emission and Field Ionisation, Vol. 9, Harvard University Press, Cambridge, MA, 1961, p. 134.
[34] F.Z. Mohamedi-Boulenouar, J. Guindet, A. Hammou, in: U. Stimming, S.C. Singhal, H. Tagawa, W. Lehnert (Eds.), Proceedings of the 5th International Symposium on Solid Oxide Fuel Cells, The Electrochemical Society Proceeding Series, The Electrochemical Society, Pennington, NJ, 1997, p. 441.
[35] D.A. Dowden, Catalysis 8 (1980) 136.
[36] W. Curtis-Conner Jr., G.M. Pajonk, S.J. Teichner, in: Advances in Catalysis, Vol. 34, Academic Press, Orlando, 1986, p. 1.
[37] A.J. Robell, E.V. Ballou, M. Boudart, J. Phys. Chem. 68 (1964) 2748.

[38] R. Kramer, M. Andre, J. Catal. 54 (1979) 287.
[39] R.D. Armstrong, B.R. Horrocks, Solid State Ionics 94 (1997) 181.
[40] V.N. Chebotin, M.V. Glumov, A.D. Neuimin, S.F. Pal'guev, Sov. Electrochem. 7 (1971) 55.
[41] B.L. Kuzin, A.D. Neuimin, S.F. Pal'guev, Sov. Electrochem. 9 (1973) 13.
[42] H. Uchida, M. Yoshida, M. Watanabe, in: M. Dokiya, O. Yamamoto, H. Tagawa, S.C. Singhal (Eds.), Proceedings of the 4th International Symposium on Solid Oxide Fuel Cells, The Electrochemical Society Proceedings Series, The Electrochemical Society, Pennington, NJ, 1995, p. 712.
[43] H. Itoh, T. Yamamoto, M. Mori, T. Horita, N. Sakai, H. Yokokawa, M. Dokiya, J. Electrochem. Soc. 144 (1997) 641.